Nanoscale

PAPER

View Article Online
View Journal | View Issue

Cite this: *Nanoscale*, 2025, **17**, 27407

Remarkably enhanced luminol chemiluminescence with a manganese porphyrin-based metal–organic framework for the sensitive detection of dopamine

Jiyang Liu,[a,b] Hongzhan Liu,[a,b] Yutong Liu,[a,b] Hao Jiang,[a] Morteza Hosseini,[a,c] Cunqi Wu*[a] and Guobao Xu *[a,b]

Received 7th September 2025,
Accepted 27th October 2025

DOI: 10.1039/d5nr03777h

rsc.li/nanoscale

The unique redox transition between Mn(III)-porphyrin and Mn(IV)-porphyrin centers confers exceptional catalytic properties to Mn-porphyrinic frameworks. In this study, we synthesized Mn-based metal–organic frameworks (Mn-MOFs) *via* a facile one-pot method using manganese(II) chloride tetrahydrate and 5,10,15,20-tetrakis(4-carboxyphenyl)porphyrin (TCPP) as the ligand. The resulting Mn-MOFs exhibited unprecedented peroxidase-mimetic activity, enhancing luminol/H_2O_2 chemiluminescence (CL) by over 1200-fold. Capitalizing on the selective quenching effect of dopamine on the Mn-MOFs/luminol/H_2O_2 system, we developed a rapid CL analytical strategy with a linear detection range of 5–1000 nM and a detection limit of 3.95 nM (S/N = 3). Furthermore, this method was successfully applied for the quantitative determination of dopamine in serum samples, achieving a recovery rate of 98.3%–104.4%. These findings highlight the potential of Mn-porphyrin-based MOFs as efficient catalysts in CL detection platforms, paving the way for their broader application in bioanalytical sensing.

1. Introduction

Chemiluminescence (CL) refers to the emission of light from a chemically excited species during a reaction.[1] Luminol, a widely used CL luminophore, was first introduced in the early 20th century.[2] Its striking ability to emit light upon oxidation in the presence of a catalyst has made it invaluable in various fields, particularly in analytical chemistry and forensic science.[3] The luminol-based CL system offers several advantages, including a broad linear detection range and the capability to operate without expensive instrumentation.[4] However, the inherently low luminous efficiency of traditional luminol/H_2O_2 CL systems remains a critical limitation, necessitating the development of highly efficient CL catalysts.[5,6]

Metal–organic frameworks (MOFs), constructed through coordination bonds between metallic nodes and organic ligands, constitute a highly porous class of materials characterized by exceptional surface areas, tunable architectures, and abundant functional sites.[5,6] These attributes make MOFs ideal platforms for designing advanced catalytic systems.[7,8] Among diverse metal–organic frameworks, porphyrin-based MOFs uniquely inherit the extensive π-conjugated architecture and outstanding catalytic properties of porphyrin macrocycles.[9] These framework materials exhibit superior catalytic activities owing to their abundant exposed active sites and uniform dispersion of catalytic sites.[10,11] Moreover, the porphyrin-metal junctions act as efficient electron transport pathways, enhancing charge transfer kinetics.[12] Recent studies have demonstrated the versatility of Mn-porphyrin MOFs in diverse applications. For instance, Liu *et al.* reported a chemiresistive sensor for NO based on Mn-porphyrin MOFs doped with Bi nanoparticles,[13] while Wan *et al.* designed a Mn(III)-sealed MOF nanosystem with a porphyrin-based ligand for redox-unlocked tumor theranostics.[14] The reversible one-electron oxidation between Mn(III) porphyrin and Mn(IV) porphyrin endows Mn-porphyrin MOFs with a high catalytic activity.[15] However, most research has focused on tumor therapy,[14,16] and their potential for chemiluminescence applications remains largely unexplored.

Dopamine (DA) is a crucial neurotransmitter in the human brain that plays a vital role in regulating numerous physiological processes, including mood, motivation, reward, and motor control.[17] It is involved in neural pathways that affect cognitive functions, emotions, and behavior.[18] Dysregulation of DA levels has been implicated in several neurological and psychia-

[a]*State Key Laboratory of Electroanalytical Chemistry, Changchun Institute of Applied Chemistry, Chinese Academy of Sciences, 5625 Renmin Street, Changchun, Jilin 130022, China. E-mail: guobaoxu@ciac.ac.cn, wucunqi@ciac.ac.cn*
[b]*School of Applied Chemistry and Engineering, University of Science and Technology of China, Hefei, Anhui 230026, China*
[c]*Nanobiosensors Lab, Department of Nanobiotechnology and Biomimetics, School of Life Science Engineering, College of Interdisciplinary Science and Technology, University of Tehran, Tehran, Iran*

tric disorders, including Parkinson's disease, schizophrenia, and depression.[19,20] Consequently, the precise and sensitive detection of DA is essential for advancing our understanding of its role in health and disease.

Despite the promising catalytic properties of Mn-porphyrin MOFs, their application in CL systems remains largely unexplored, especially when compared to their use in other fields such as tumor therapy and gas sensing.[21] Furthermore, although various MOFs have been developed for DA sensing, achieving high sensitivity in a simple CL system remains a challenge.[22,23] Moreover, the intricate synthetic conditions often associated with these materials can hinder their widespread application.

In this study, a manganese-based MOF (Mn-MOF) was synthesized *via* a one-pot method and applied for CL analysis for the first time. A marked enhancement in the CL intensity of the luminol/H_2O_2 system was observed. The potential mechanism for this enhancement was subsequently investigated using UV-visible absorption spectroscopy, CL spectroscopy, radical scavenger experiments, and 3,3′,5,5′-tetramethylbenzidine (TMB) chromogenic reaction. After the addition of DA, a significant decrease in the CL intensity of the system was observed, demonstrating high selectivity for DA detection. This study establishes a simple, rapid, and highly sensitive method for the quantitative determination of DA.

2. Experimental section

2.1. Materials

5,10,15,20-Tetrakis (4-carboxyphenyl)porphyrin (TCPP) was purchased from Heowns Biochem Technologies (Tianjin, China) (97% purity). Triethylamine (Et_3N), *N*,*N*-dimethylacetamide (DMA), thiourea (TU), manganese(II) chloride tetrahydrate ($MnCl_2{\cdot}4H_2O$), and hydrogen peroxide (H_2O_2) were obtained from Xilong Chemical Co., Ltd (Guangdong, China). Luminol (5-amino-2,3-dihydrophthalazine-1,4-dione) was sourced from Ark Pharm (USA). 3,3′,5,5′-Tetramethyl-benzidine (TMB) was provided by Sinopharm Chemical Reagent Co., Ltd (Shanghai, China). Ascorbic acid (AA) and uric acid (UA) were acquired from Shanghai Macklin Biochemical Co., Ltd (Shanghai, China). L-Histidine (His) was purchased from TCL. DA hydrochloride and other amino acids were acquired from Aladdin (Shanghai, China). Sodium azide (NaN_3) and superoxide dismutase (SOD) were supplied by Beijing HWRK Chem. Co., Ltd (Beijing, China) and Tianjin Fuchen Chemical Reagent Factory (Tianjin, China), respectively. The bovine serum samples were obtained from Zhejiang TianHang Biotechnology Co. Ltd. A 10 mM luminol stock solution was prepared by dissolving 0.1772 g of luminol in 100 mL of 0.1 M NaOH aqueous solution, and the resulting mixture was stored in the dark at 4 °C for at least one week prior to use. Phosphate buffer solutions with different pH values were prepared by using NaH_2PO_4, Na_2HPO_4, and Na_3PO_4. All chemicals were analytical-grade reagents, and all experimental solutions were prepared with Millipore-purified water.

2.2. Apparatus

The CL signals were measured using a flow injection analysis-based chemiluminescence system (FIA-CL), comprising an IFIS-C mode intelligent flow injection sampler (Xi'an Mindray Electronic Technology Co., Ltd, Xi'an, China), a BPCL ultra-weak luminescence analyzer (Institute of Biophysics, Chinese Academy of Sciences), and a self-assembled flow cell. The photomultiplier tube (PMT) voltage was set to −420 V. Scanning electron microscopy (SEM) analysis was conducted using an XL30 ESEM microscope. Transmission electron microscopy (TEM) imaging and energy-dispersive X-ray (EDX) spectroscopy were performed using a Hitachi 600 microscope. X-ray diffraction (XRD) analysis was performed using a Bruker D8 Advanced diffractometer equipped with a Cu Kα radiation filter. X-ray photoelectron spectroscopy (XPS) measurements were conducted using a Thermo Scientific ESCALAB 250Xi spectrometer with Al Kα radiation serving as the excitation source. Fourier transform infrared spectra (FT-IR) were measured using a Bruker VERTEX 70 spectrometer. The UV-vis absorption spectra were recorded using a Shimadzu UV-2600 spectrophotometer. CL spectra were measured with an HRS-300-SpectraPro (Princeton Instruments, USA). Electron spin resonance (ESR) spectra were recorded at room temperature with an EMXPlus (Bruker, Germany) spectrometer.

2.3. Preparation of Mn-MOFs

Mn-MOFs were synthesized using a simple one-pot approach with slight modifications based on previously reported methods.[24] Initially, 3 mL of methanol (MeOH) and 25 mL of DMA were mixed in a flask. A solution containing $MnCl_2{\cdot}4H_2O$ (200 mg), TCPP (100 mg), and Et_3N (3 mL) was ultrasonically dissolved and then added to the mixture. The resulting solution was magnetically stirred and refluxed at 100 °C for 24 hours. After natural cooling, the reaction mixture was centrifuged at 8500 rpm for 5 min, and the precipitate was collected and washed sequentially with 1 M HCl (once), water (three times), and acetone (three times). The wet product was then dried under vacuum at 40 °C overnight.

2.4. Evaluation of the peroxidase-like catalytic performance of Mn-MOFs in the luminol/H_2O_2 CL reaction

Utilizing the designed FIA-CL platform, the CL performance of the luminol/H_2O_2/Mn-MOFs system was characterized. As illustrated in Scheme S1, the solution was pumped at a flow rate of 2.5 mL min^{-1} through flow paths I, II, and III, where flow path I contained H_2O_2, flow path II contained luminol, and flow path III was PBS solution. A 50 μg mL^{-1} Mn-MOF solution was introduced into flow path III using a loop injector. Subsequently, the CL signal was monitored using a BPCL ultra-weak luminescence analyzer.

2.5. Procedure for DA detection

Different concentrations of DA were combined with the Mn-MOFs and injected into the system *via* a loop injector. The resulting CL intensities were subsequently measured using a

BPCL ultraweak luminescence analyzer. The final concentration of Mn-MOFs was maintained at 50 μg mL^{-1}.

2.6. DA analysis in real samples

The developed method was further applied for the analysis of DA in real serum samples. Initially, bovine serum was diluted 1000-fold with normal saline (0.9% NaCl). The diluted sample was then combined with the Mn-MOFs solution and injected into the flow channel for analysis.

3. Results and discussion

3.1. Characterization of Mn-MOFs

After synthesizing the Mn-MOFs, various characterization techniques were employed to analyze their structural and morphological properties. The SEM images and TEM images in Fig. 1 show rhombic lamellar MOFs with approximately 1 μm in length and 275 nm in width. In addition, TEM mapping images and EDX (Fig. 1d–i) results revealed the homogeneous distribution of C, N, O and Mn elements in the Mn-MOFs.

Subsequently, the XRD patterns and FT-IR spectra of the Mn-MOFs were obtained for further characterization. From the observation of the XRD patterns in Fig. S1, Mn-MOFs presented a set of characteristic peaks that differed from the peaks of the precursors (TCPP and $MnCl_2{\cdot}4H_2O$) but were similar to the pattern of the single crystal previously reported.[14] As illustrated in Fig. 2a, the transmission of C═O stretching vibration at 1715 cm^{-1} was shifted, suggesting the formation of a rigid structure connected by hydrogen bonds in the Mn-MOFs.[24,25] Moreover, the coordination bond between N and Mn atoms resulted in a new peak at 1012 cm^{-1}, corres-

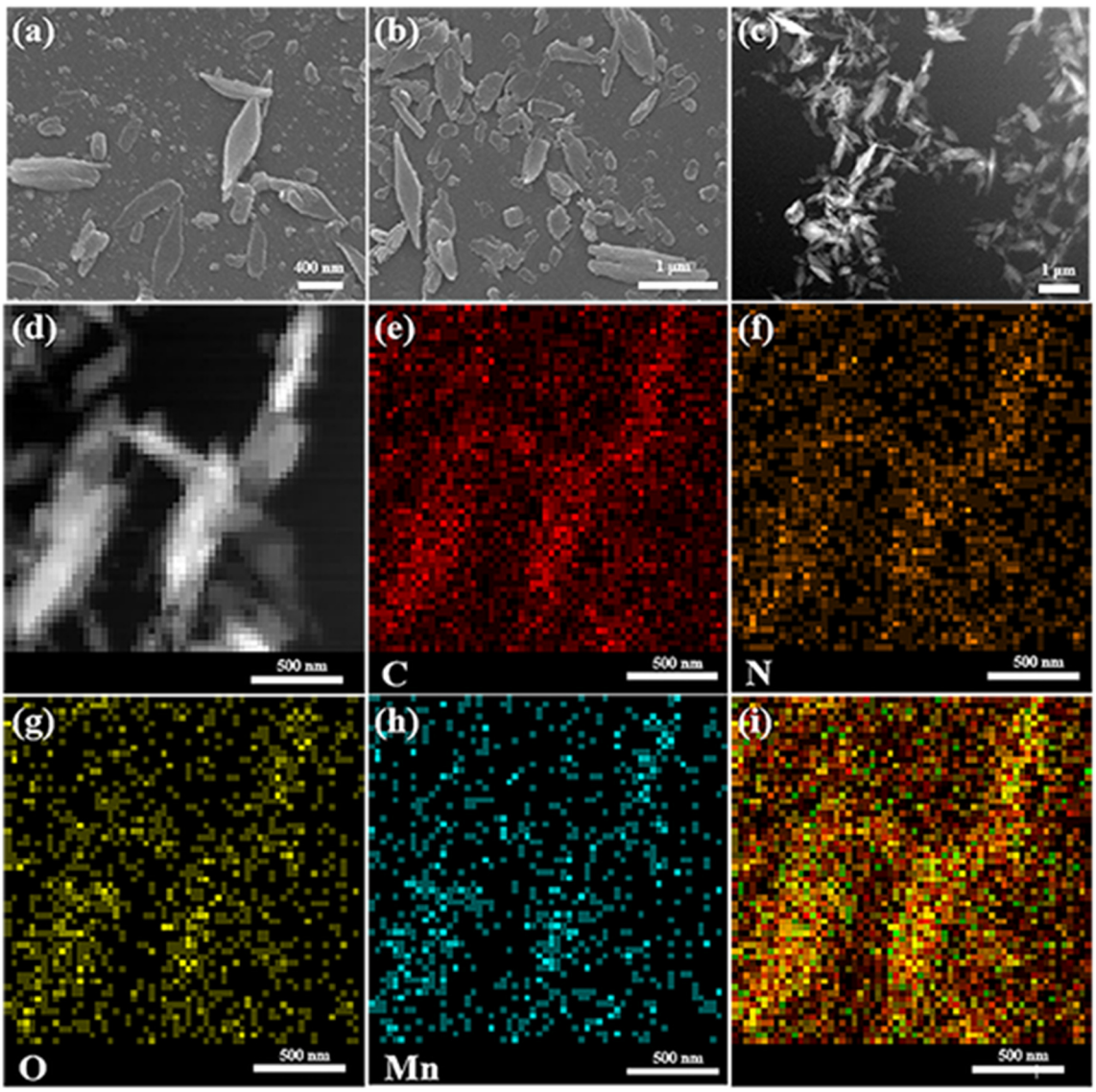

Fig. 1 SEM (a and b) and TEM (c) images of the synthesized Mn-MOFs at different scale bars. TEM image (d) and the corresponding EDX elemental-mapping images (e–i) for C, N, O, Mn and C/N/O/Mn with color superposition, respectively.

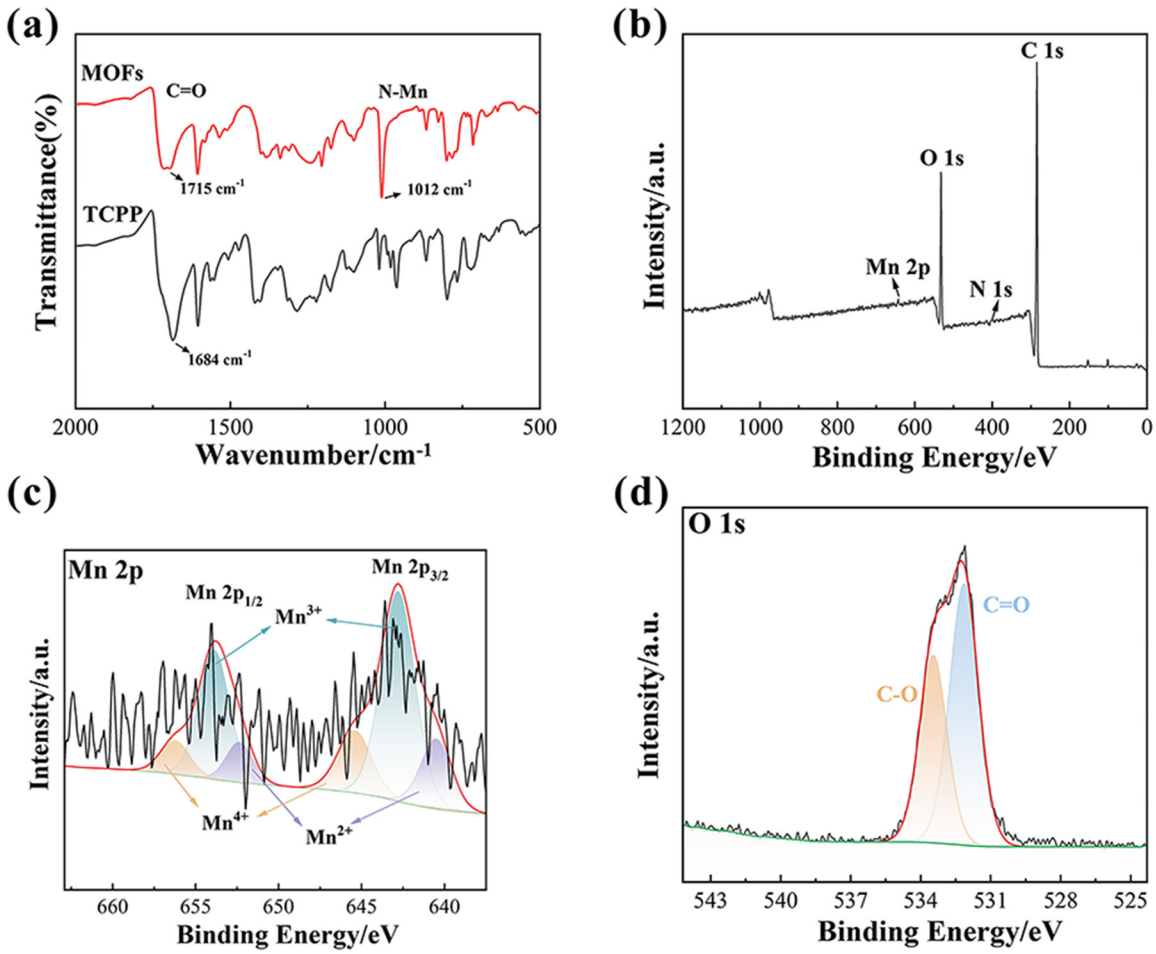

Fig. 2 (a) FT-IR spectra of Mn-MOFs. Full-scan (b) and high-resolution XPS spectra for Mn (c) and O (d) of Mn-MOFs.

ponding to the N–Mn stretching vibration. XPS analysis further verified the presence of C, N, O, and Mn in the Mn-MOFs (Fig. 2b–d). Meanwhile, the binding energies observed in the XPS spectra (Fig. 2c) at 645.28, 642.66 and 640.51 eV, corresponding to the $2p_{3/2}$ levels of Mn(IV), Mn(III) and Mn(II) ions, respectively, are consistent with previously reported values.[25,26] The synthesis reaction was carried out under aerobic conditions. The basic reaction environment created by Et_3N facilitates the oxidation of Mn(II) to Mn(III) by dissolved oxygen, leading to the generation of Mn(III) and Mn(IV).[27,28]

3.2. CL reaction and mechanism of luminol/H_2O_2 with Mn-MOFs

To investigate the catalytic effect of Mn-MOFs in the luminol/H_2O_2 system, we systematically analyzed the CL kinetic curves of luminol/H_2O_2 and luminol/H_2O_2/Mn-MOFs. As illustrated in Fig. 3a, the addition of Mn-MOFs increases the CL intensity by more than 1200-fold, demonstrating the superior catalytic activity of the Mn-MOFs. To elucidate the underlying mechanism, we further characterized the CL and UV-vis absorption spectra of the system. Fig. 3b and c reveal that the maximum CL emission wavelength remained constant at 450 nm regardless of the presence of the Mn-MOFs, while the UV-vis absorption spectrum of the luminol/Mn-MOFs system corresponded to the superposition of the individual component spectra. These findings conclusively indicate that the Mn-MOFs neither form new luminescent complexes with luminol nor alter the intrinsic emitter species.[29] Instead, they accelerate the catalytic oxidation of luminol by H_2O_2 to generate the excited-state 3-aminophthalate (3-APA*), aligning with established catalytic pathways reported for luminol/H_2O_2 CL systems.[3,6] Thus, the CL enhancement is attributed to the exceptional catalytic efficiency of Mn-MOFs. Furthermore, the peroxidase-mimetic activity of Mn-MOFs was validated through a TMB chromogenic assay (Fig. 3d). The material effectively catalyzed H_2O_2 decomposition to produce hydroxyl radicals, which subsequently oxidized TMB to form a blue-colored oxTMB product with a characteristic absorption maximum at 652 nm.[30]

To investigate free radical production in the luminol/H_2O_2/Mn-MOFs system, ESR studies were conducted. As shown in Fig. S2, ESR signals were observed using specific spin trapping agents. In the presence of 5,5-dimethyl-1-pyrroline *N*-oxide (DMPO), characteristic signals corresponding to the

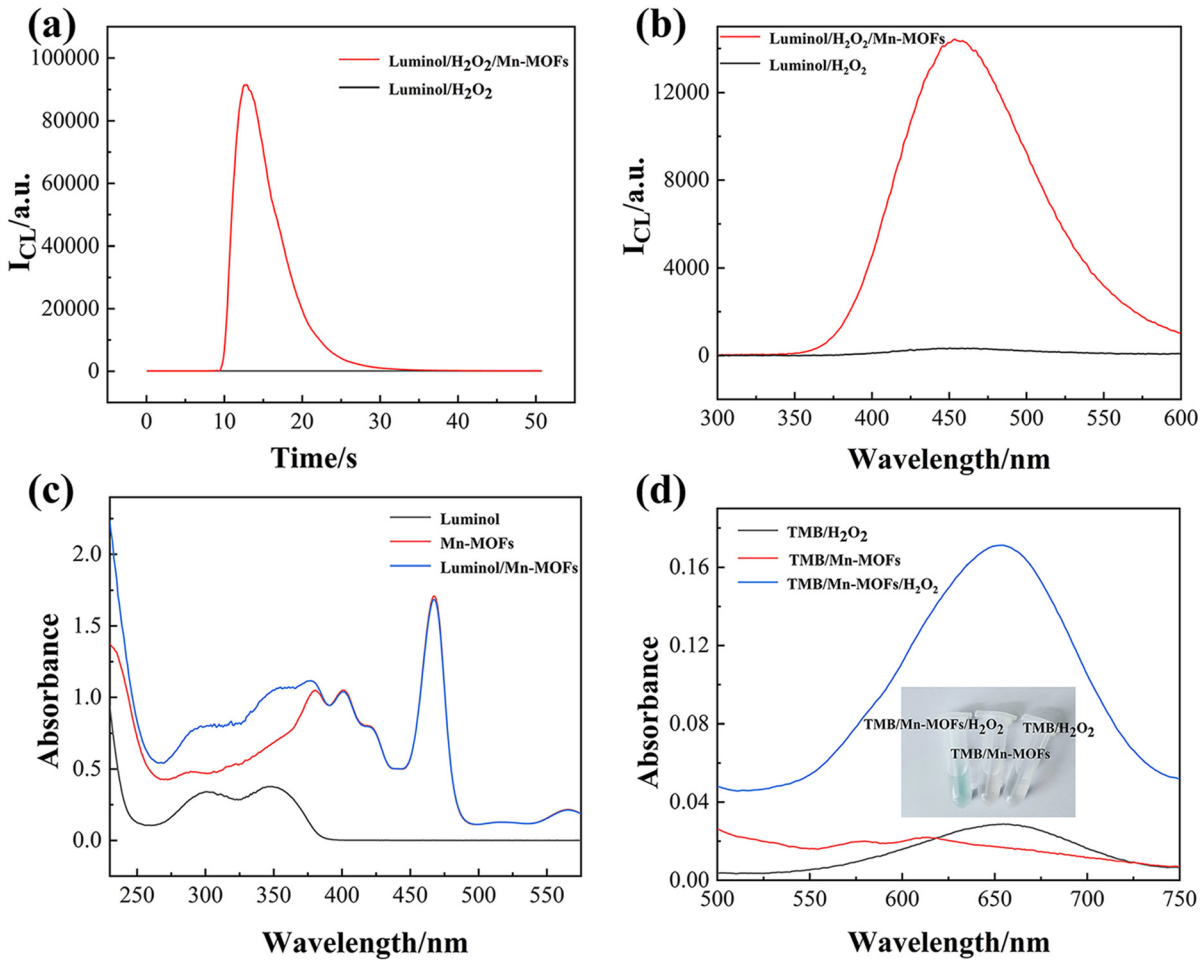

Fig. 3 (a) CL intensity–time curves and (b) CL spectra of the luminol/H_2O_2 system in the absence (black line) and presence (red line) of Mn-MOFs. Reaction conditions: 50 μM luminol in PBS (pH 11.0), 2000 μM H_2O_2, and 50 μg mL^{-1} Mn-MOFs. (c) UV-vis absorption spectra of luminol (black line), Mn-MOFs (red line), and luminol/Mn-MOFs (blue line). (d) UV-vis absorption spectra of TMB/H_2O_2 (black line), TMB/Mn-MOFs (red line), and TMB/Mn-MOFs/H_2O_2 (blue line) in a 0.2 M HAc/NaAc buffer solution (pH 4.0). Inset: images captured after 2 hours (left to right): TMB/Mn-MOFs/H_2O_2, TMB/Mn-MOFs, and TMB/H_2O_2. Reaction conditions: 1 mM TMB, 100 mM H_2O_2, and 10 μg mL^{-1} Mn-MOFs.

DMPO-$OH^{\bullet}$ and DMPO-$O_2^{\bullet-}$ adducts were detected. Furthermore, a typical triplet signal for the TEMPO adduct was recorded using 2,2,6,6-tetramethyl-4-piperidinone (TEMP) as a trap for $^1O_2$.[31] These ESR results indicate that the Mn-MOFs effectively catalyze the decomposition of H_2O_2 to generate $OH^{\bullet}$, $O_2^{\bullet-}$, and $^1O_2$.

To evaluate the relative contribution of each ROS, a series of radical scavenging experiments was conducted. As illustrated in Fig. 4, the addition of superoxide dismutase (SOD), an $O_2^{\bullet-}$ scavenger, caused a significantly attenuated CL emission, indicating non-negligible involvement of superoxide radicals. In contrast, the addition of NaN_3, a $^1O_2$ scavenger, had a negligible impact on CL intensity. Most critically, the addition of thiourea (TU), a specific $OH^{\bullet}$ scavenger, resulted in a dramatic reduction in CL intensity, indicating that $OH^{\bullet}$ plays an important role in the CL process.

Based on these findings, we propose a plausible CL mechanism (Fig. 5). H_2O_2 is rapidly decomposed into $OH^{\bullet}$ and $O_2^{\bullet-}$ through catalytic action in the presence of the peroxidase-like Mn-MOFs material. Subsequently, under alkaline conditions, $OH^{\bullet}$ and $O_2^{\bullet-}$ react with the luminol anion to form the excited-state intermediate 3-APA*.[32,33] Finally, the radiative decay of 3-APA* to its ground state results in the emission of CL.

3.3. Optimization of experimental conditions

The CL of luminol exhibits strong pH dependence, with optimal emission occurring under alkaline conditions. As shown in Fig. S3, the experimental conditions were methodically optimized to achieve maximal CL enhancement at pH 11.0 within the tested range of 8.0–12.5. Under these optimized conditions, the luminol concentration was maintained at 50 μmol L^{-1} based on CL enhancement efficiency. Subsequently, the effects of H_2O_2 and Mn-MOFs concentrations on the CL intensity were examined. Following the principle of maximizing CL enhancement while conserving reagents, 2000 μmol L^{-1} H_2O_2 and 50 μg mL^{-1} Mn-MOFs were identified as optimal. The optimized system exhibited stable and reproducible luminescence signals, with a relative stan-

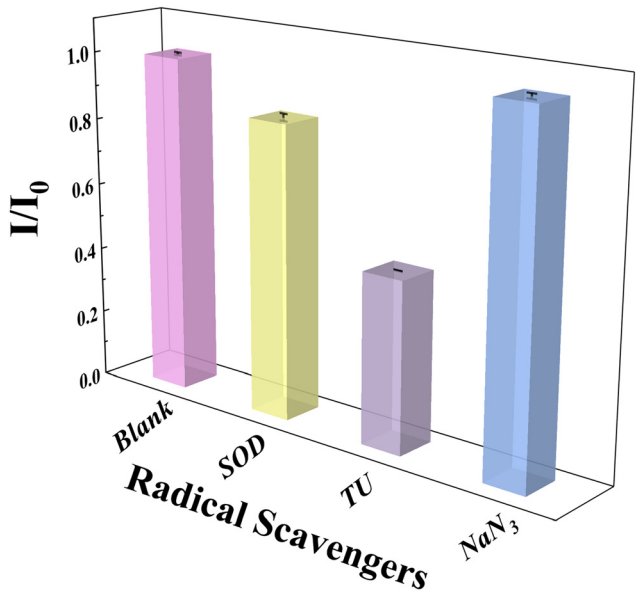

Fig. 4 Relative CL intensity (I/I_0) of the luminol/H_2O_2/Mn-MOFs system in the presence of 1.0 μg mL^{-1} SOD, 1.0 mM TU, and 1.0 mM NaN_3, respectively. I_0 represents the initial intensity and I represents the intensity with scavengers. Reaction conditions: 50 μM luminol in PBS (pH 11.0), 2000 μM H_2O_2, and 50 μg mL^{-1} Mn-MOFs.

dard deviation (RSD) of 1.11% for nine consecutive measurements (Fig. S4).

3.4. Detection of DA

The CL-based DA detection system was tested under the optimized conditions. As shown in Fig. 6a, the CL signal gradually decreased with the increase of DA concentration from 5 nM to 1 μM. As shown in Fig. 6b, a linear correlation was observed between the logarithm of the CL intensity and the DA concentration, expressed as $\log(I_{CL}) = 5.04–1.39 \times 10^{-4}c$ ($R^2 = 0.998$). With a 3.95 nM detection limit (S/N = 3), this method surpasses previous approaches in both detection range and sensitivity, as shown in Table 1.

3.5. Selectivity for DA detection

The selectivity of the DA detection was evaluated against potential interferents in biological matrices. Various coexisting substances, including ascorbic acid (AA), uric acid (UA), norepinephrine (NE), glucose, and amino acids, were examined to evaluate their impact on the CL response. As shown in Fig. 7, the CL signal was significantly quenched upon addition of 0.5 μM DA, whereas common coexisting interferents at equivalent or higher concentrations caused negligible changes in the CL

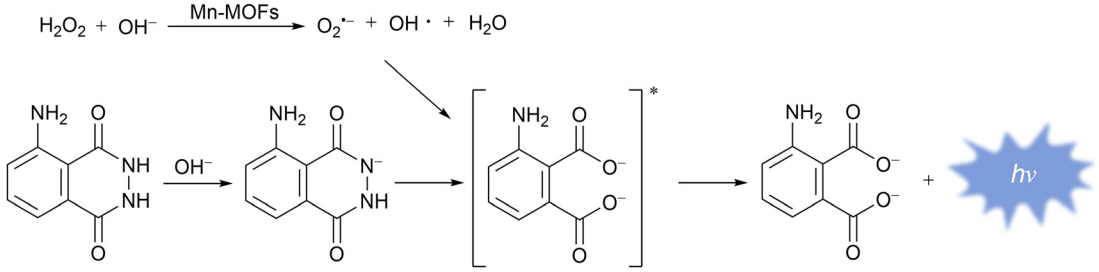

Fig. 5 Mechanism of the luminol/H_2O_2/Mn-MOFs CL system.

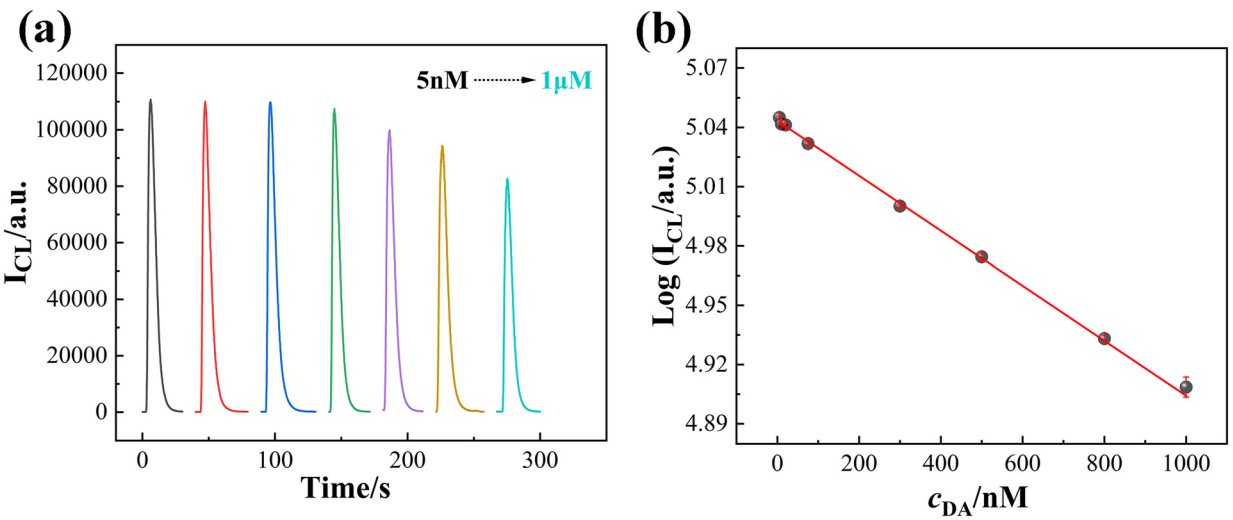

Fig. 6 (a) CL emission–time curves at different concentrations of DA. (b) Linear relationship between the log of CL peak intensity and the concentration of DA from 5 to 1000 nM. Experimental conditions: 50 μM luminol in PBS (pH 11.0), 2000 μM H_2O_2, and 50 μg mL^{-1} Mn-MOFs.

Table 1 Comparison of different methods for the detection of DA

Analytical method	Materials	Linear range (μM)	LOD (nM)	Real sample	Ref.
Fluorescence	UiO-66-NH_2 MOF	1–70	570	Human serum	34
Fluorescence	ECP nanoflakes	0.1–10	21	Human serum	35
Fluorescence	Eu-MOF	0–500	15	Human serum	36
Electrochemistry	CoNi-MOF	0.1–400	86	Human serum	37
Electrochemistry	Pd_3-NiFe MOF/NF	1–10	0.068	Artificial cerebrospinal fluid	38
Electrochemistry	Fe_3O_4@ZIF-8@AuNPs	0.05–120	26	PC12 cells	39
ECL	Zn-tpMOF	0.01–1000	8.2	Human serum	40
CL	Fe/Co-MOF NSs	50–800	20.88	Human serum	29
CL	Fe-MOXs	0.05–0.6	20.4	Standard solution	41
CL	Mn-MOFs	0.005–1	3.95	Bovine serum	This work

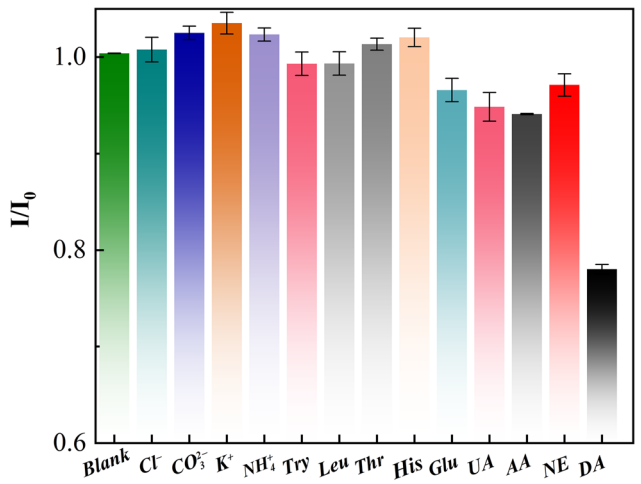

Fig. 7 Selectivity of the DA detection. I_0 represents the initial intensity and I represents the intensity with interfering species. Reaction conditions: the concentration of all the metal ions is 0.2 mM, the concentration of all the amino acids and glucose are 0.5 μM, and the concentrations of DA, NE, AA, and UA are 0.5 μM, 50 μM luminol in PBS (pH 11.0), 2000 μM H_2O_2, and 50 μg mL^{-1} Mn-MOFs.

signal. These results demonstrate the excellent selectivity of the luminol/H_2O_2/Mn-MOFs-based CL sensor for DA detection.

3.6. DA analysis in serum samples

To assess the analytical practicality of the developed CL detection system, a standard addition method was conducted. The bovine serum was first diluted 1000-fold in normal saline to mitigate biological matrix interference. As summarized in Table S1, the recoveries ranged from 98.3% to 104.4%, confirming the potential of the CL detection strategy for real-sample quantification. However, it is necessary to couple with separation techniques (*e.g.* HPLC) to further improve selectivity for clinical analysis.

4. Conclusions

This study presents the first demonstration of Mn-MOFs with peroxidase-like activity for enhancing luminol/H_2O_2 CL. A novel flow injection analysis sensing platform was developed based on the luminol/H_2O_2/Mn-MOFs system, achieving high sensitivity for DA detection through its distinctive CL quenching mechanism. The system exhibits a logarithmic correlation (5 nM–1 μM range) between CL intensity and DA concentration (R^2 = 0.998), with a detection limit of 3.95 nM. These results highlight the promising analytical applications of Mn-MOFs-based CL. The approach may be coupled with microfluidic platforms and portal CL detectors (*e.g.* smart phones) to develop automated, high-throughput, and miniaturized analysis systems for point-of-care testing.

Author contributions

Jiyang Liu: writing – original draft preparation, methodology, investigation, formal analysis, conceptualization. Hongzhan Liu: methodology. Yutong Liu: investigation, formal analysis. Hao Jiang: writing – review and editing. Morteza Hosseini: writing – review and editing. Cunqi Wu: supervision. Guobao Xu: writing – review and editing, resources, funding acquisition, supervision.

Conflicts of interest

The authors have no competing interests to declare that are relevant to the content of this article.

Data availability

The data supporting this article have been included as part of the supplementary information (SI). Supplementary information is available. Schematic diagram of the detection system based on the FIA-CL, XRD patterns, ESR spectra, Optimization of CL response through parameter modulation, System stability test, Results of the determination of DA in actual samples. See DOI: https://doi.org/10.1039/d5nr03777h.

Acknowledgements

This work was financially supported by the National Natural Science Foundation of China (22174136) and the CAS President's International Fellowship Initiative (PIFI).

References

1 L. Zhao, J. Xu, L. Xiong, S. Wang, C. Yu, J. Lv and J.-M. Lin, Recent Development of Chemiluminescence for Bioanalysis, *TrAC, Trends Anal. Chem.*, 2023, **166**, 117213.
2 H. O. Albrecht, Über Die Chemiluminescenz Des Aminophthalsäurehydrazids, *Z. Phys. Chem.*, 1928, **136U**, 321–330.
3 Y. Jiang, X. Yang, S. Li, Y. Qiao, Y. Zhou and Y. Li, Chemiluminescence Initiated by Nebulization of Oxidant- and Catalyst-Free Aqueous Luminol Solutions, *Chem. Eng. J.*, 2024, **481**, 148753.
4 S. Tian, C. Peng, H. Xing, Y. Xue, J. Li and E. Wang, Boosting Photon Emission from the Chemiluminescence of Luminol Based on Host–Guest Recognition for the Determination of Dopamine, *Anal. Chem.*, 2024, **96**, 514–521.
5 I. M. Mostafa, A. Abdussalam, H. Liu, Z. Dong, S. Xia, A. a. M. A. Alboull, B. Lou and G. Xu, Signal-on Detection of Dopamine and Tyrosinase Using Tris(Hydroxypropyl) Phosphine as a New Lucigenin Chemiluminescence Coreactant, *Anal. Chem.*, 2024, **96**, 14741–14748.
6 H. Gao, T. Sun, W. Wang, J. Li, M. Zhang, Y. Hou and G. Bai, Self-Illuminating Copper-Luminol Coordination Polymers for Bioluminescence Imaging of Oxidative Damage, *Anal. Chem.*, 2024, **96**, 16434–16442.
7 S. Larijani, A. Zarepour, A. Khosravi, S. Iravani, M. Eskandari and A. Zarrabi, Advancing Paper-Based Sensors with Mxenes and MOFs: Exploring Cutting-Edge Innovations, *J. Mater. Chem. A*, 2025, **13**, 158–183.
8 J. Liu, L. Geng, H. Wang, J. Huang, G. Wang, Z. Shen, M. Hu, B. Li, J. Sun, J. Dong, Y. Guo and X. Sun, Detection of Acetamiprid Residues in Vegetables by a Self-Enhanced Bimetallic Luminescent MOF-Based Electrochemiluminescence-Electrochemistry Dual-Mode Aptasensor, *Sens. Actuators, B*, 2024, **410**, 135665.
9 P. Gao, S. Mukherjee, M. Z. Hussain, S. Ye, X. Wang, W. Li, R. Cao, M. Elsner and R. A. Fischer, Porphyrin-Based MOFs for Sensing Environmental Pollutants, *Chem. Eng. J.*, 2024, **492**, 152377.
10 S. Zhu, X. Lin, P. Ran, Q. Xia, C. Yang, J. Ma and Y. Fu, A Novel Luminescence-Functionalized Metal-Organic Framework Nanoflowers Electrochemiluminesence Sensor Via "on-off" System, *Biosens. Bioelectron.*, 2017, **91**, 436–440.
11 L. Zheng, Q. Guo, C. Yang, J. Wang, X. Xu and G. Nie, Electrochemiluminescence and Photoelectrochemistry Dual-Signal Immunosensor Based on $Ru(bpy)_3^{2+}$-Functionalized MOF for Prostate-Specific Antigen Sensitive Detection, *Sens. Actuators, B*, 2023, **379**, 133269.
12 J. Ma, G. Chen, W. Bai and J. Zheng, Amplified Electrochemical Hydrogen Peroxide Sensing Based on Cu-Porphyrin Metal-Organic Framework Nanofilm and G-Quadruplex-Hemin Dnazyme, *ACS Appl. Mater. Interfaces*, 2020, **12**, 58105–58112.
13 Q. Liu, Y. Zhang, Q. Sun, H. Li, W. Chen, S. Yu and Y. Chen, High-Performance Specific Detection of NO_2 Based on PCN-222-Mn Doped with Bi Electron Mediator, *Sens. Actuators, B*, 2024, **399**, 134865.
14 S.-S. Wan, Q. Cheng, X. Zeng and X.-Z. Zhang, A Mn(III)-Sealed Metal-Organic Framework Nanosystem for Redox-Unlocked Tumor Theranostics, *ACS Nano*, 2019, **13**, 6561–6571.
15 Y. Chen, H. Zhong, J. Wang, X. Wan, Y. Li, W. Pan, N. Li and B. Tang, Catalase-Like Metal-Organic Framework Nanoparticles to Enhance Radiotherapy in Hypoxic Cancer and Prevent Cancer Recurrence, *Chem. Sci.*, 2019, **10**, 5773–5778.
16 H. Zhang and X.-B. Yin, Mixed-Ligand Metal-Organic Frameworks for All-in-One Theranostics with Controlled Drug Delivery and Enhanced Photodynamic Therapy, *ACS Appl. Mater. Interfaces*, 2022, **14**, 26528–26535.
17 R. A. Wise and C. J. Jordan, Dopamine, Behavior, and Addiction, *J. Biomed. Sci.*, 2021, **28**, 83.
18 R. A. Wise and M. A. Robble, Dopamine and Addiction, *Annu. Rev. Psychol.*, 2020, **71**, 79–106.
19 Y. Cai, B. E. Nielsen, E. E. Boxer, J. Aoto and C. P. Ford, Loss of Nigral Excitation of Cholinergic Interneurons Contributes to Parkinsonian Motor Impairments, *Neuron*, 2021, **109**, 1137–1149.
20 B. Channer, S. M. Matt, E. A. Nickoloff-Bybel, V. Pappa, Y. Agarwal, J. Wickman and P. J. Gaskill, Dopamine, Immunity, and Disease, *Pharmacol. Rev.*, 2023, **75**, 62–158.
21 H. Qu, L. Hang, Y. Diao, H. Wang, L. Fang, W. Liu, J. Liu, H. Sun, J. Wang, X. Meng, H. Li and G. Jiang, Mn-Doped MOF Nanoparticles Mitigating Hypoxia Via *in situ* Substitution Strategy for Dual-Imaging Guided Combination Treatment of Microwave Dynamic Therapy and Chemotherapy, *J. Colloid Interface Sci.*, 2025, **685**, 912–926.
22 W. Cai, L. Yin, Y. Shi, H. Zhang, D. Wu, J. Li, L. Xu and Y. Kong, An Ultrasensitive Electrochemiluminescence Sensor for Dopamine Based on Dual-Ligand Eu MOF with Cu_2O Nanocrystals as a Co-Reactant Accelerator, *Sens. Actuators, B*, 2025, **443**, 138278.
23 Y. Zhang, E. Gao and V. P. Fedin, Molybdenum Disulfide-Filled Double-Sandwiched Cd-MOF for the Quantitative Detection of Nanomolar Acetaminophen and Dopamine in Pharmaceuticals, *Chem. Eng. J.*, 2024, **498**, 155469.
24 J. Ya, H. Zhang, G. Qin, C. Huang, C. Zhao, J. Ren and X. Qu, A Biocompatible Hydrogen-Bonded Organic Framework (HOF) as Sonosensitizer and Artificial Enzyme for in-Depth Treatment of Alzheimer's Disease, *Adv. Healthcare Mater.*, 2024, **13**, 2402342.
25 K. Yu, P. Puthiaraj and W.-S. Ahn, One-Pot Catalytic Transformation of Olefins into Cyclic Carbonates over an Imidazolium Bromide-Functionalized Mn(III)-Porphyrin Metal-Organic Framework, *Appl. Catal., B*, 2020, **273**, 119059.
26 Y. Du, Z. Hua, W. Huang, M. Wu, M. Wang, J. Wang, X. Cui, L. Zhang, H. Chen and J. Shi, Mesostructured Amorphous Manganese Oxides: Facile Synthesis and Highly Durable Elimination of Low-Concentration NO at Room Temperature in Air, *Chem. Commun.*, 2015, **51**, 5887–5889.

27 J. J. Morgan, M. A. Schlautman and H. Bilinski, Rates of Abiotic MnII Oxidation by O_2: Influence of Various Multidentate Ligands at High pH, *Environ. Sci. Technol.*, 2021, **55**, 14426–14435.

28 D. Diem and W. Stumm, Is Dissolved Mn^{2+} Being Oxidized by O_2 in Absence of Mn-Bacteria or Surface Catalysts?, *Geochim. Cosmochim. Acta*, 1984, **48**, 1571–1573.

29 Y. Peng, L. Yu, M. Sheng, Q. Wang, Z. Jin, J. Huang and X. Yang, Room-Temperature Synthesized Iron/Cobalt Metal-Organic Framework Nanosheets with Highly Efficient Catalytic Activity toward Luminol Chemiluminescence Reaction, *Anal. Chem.*, 2023, **95**, 18436–18442.

30 X. Wang, X. Zang, X. Wang, W. Zhang, Y. Fang and B. Cui, Molecularly Imprinted Electrochemiluminescence-Colorimetric Dual-Mode Sensor Based on Mn@NC Nanozyme Amplification for the Detection of Phoxim, *Chem. Eng. J.*, 2024, **500**, 156817.

31 K. Ji, S. Xia, X. Sang, A. M. Zeid, A. Hussain, J. Li and G. Xu, Enhanced Luminol Chemiluminescence with Oxidase-Like Properties of FeOOH Nanorods for the Sensitive Detection of Uric Acid, *Anal. Chem.*, 2023, **95**, 3267–3273.

32 F. Liu, S. Xia, A. a. M. A. Alboull, Z. Dong, H. Liu, C. Meng, F. Wu and G. Xu, Remarkably Enhanced Luminol/H_2O_2 Chemiluminescence with Excellent Peroxidase-Like Activity of FeCoNi-Based Metal-Organic Xerogels for the Sensitive Detection of Dopamine, *Anal. Chem.*, 2023, **95**, 9380–9387.

33 J. Wang, C. Hu, Y.-s. Wang and H. Cui, Chemiluminescent Two-Dimensional Metal-Organic Framework with Multiple Metal Catalytic Centers and Its Peroxidase-Like Activity for Sensing of Small Molecules, *ACS Appl. Mater. Interfaces*, 2022, **14**, 3156–3164.

34 N. Wang, M. Xie, M. Wang, Z. Li and X. Su, UiO-66-NH_2 MOF-Based Ratiometric Fluorescent Probe for the Detection of Dopamine and Reduced Glutathione, *Talanta*, 2020, **220**, 121352.

35 F. Moghzi, J. Soleimannejad, E. C. Sañudo and J. Janczak, Dopamine Sensing Based on Ultrathin Fluorescent Metal-Organic Nanosheets, *ACS Appl. Mater. Interfaces*, 2020, **12**, 44499–44507.

36 Q. Du, P. Wu, P. Dramou, R. Chen and H. He, One-Step Fabrication of a Boric Acid-Functionalized Lanthanide Metal-Organic Framework as a Ratiometric Fluorescence Sensor for the Selective Recognition of Dopamine, *New J. Chem.*, 2019, **43**, 1291–1298.

37 Y. Zhou, M. Tian, R. Li, Y. Zhang, G. Zhang, C. Zhang and S. Shuang, Ultrasensitive Electrochemical Platform for Dopamine Detection Based on CoNi-MOF@ERGO Composite, *ACS Biomater. Sci. Eng.*, 2023, **9**, 5599–5609.

38 S. Wang, D. Wang, M. Li, S. Wang, S. Xiang, K. Feng, Q. Liu, P. Wang, Y. Li and F. Tang, Interfacial Galvanic Replacement Strategy for Pd-Doped NiFe MOF Nanosheets with Highly Efficient Dopamine Detection, *Microchim. Acta*, 2024, **191**, 280.

39 J. Guo, Y. Ma, T. Han, J. Yang and P. Miao, Magnetic MOF Composites for the Electrocatalysis and Biosensing of Dopamine Released from Living Cells, *J. Mater. Chem. B*, 2024, **12**, 8181–8188.

40 H. Fu, Z. Xu, T. Liu and J. Lei, In Situ Coordination Interactions between Metal-Organic Framework Nanoemitters and Coreactants for Enhanced Electrochemiluminescence in Biosensing, *Biosens. Bioelectron.*, 2023, **222**, 114920.

41 L. He, Z. W. Peng, Z. W. Jiang, X. Q. Tang, C. Z. Huang and Y. F. Li, Novel Iron(III)-Based Metal-Organic Gels with Superior Catalytic Performance toward Luminol Chemiluminescence, *ACS Appl. Mater. Interfaces*, 2017, **9**, 31834–31840.